# Quantum skyrmion Hall effect in *f*-electron systems

Robert Peters [1,*] Jannis Neuhaus-Steinmetz [2,3] and Thore Posske [3,4,†]

[1]*Department of Physics, Kyoto University, Kyoto 606-8502, Kyoto, Japan*

[2]*Department of Physics, University of Hamburg, 20355 Hamburg, Germany*

[3]*The Hamburg Centre for Ultrafast Imaging, Luruper Chaussee 149, 22761 Hamburg, Germany*

[4]*I. Institute for Theoretical Physics, Universität Hamburg, Notkestraße 9, 22607 Hamburg, Germany*

(Received 16 April 2023; revised 4 July 2023; accepted 7 August 2023; published 12 September 2023)

The flow of electric current through a two-dimensional material in a magnetic field gives rise to the family of Hall effects. The quantum versions of these effects accommodate robust electronic edge channels and fractional charges. Recently, the Hall effect of skyrmions, classical magnetic quasiparticles with a quantized topological charge, has been theoretically and experimentally reported, igniting ideas on a quantum version of this effect. To this end, we perform dynamical mean-field-theory calculations on localized $f$ electrons coupled to itinerant $c$ electrons in the presence of spin-orbit interaction and a magnetic field. Our calculations reveal localized quantum nanoskyrmions that start moving transversally when a charge current in the itinerant electrons is applied. The results show the time-transient buildup of the quantum skyrmion Hall effect, accompanied by an Edelstein effect and a magnetoelectric effect that rotate the spins. This work motivates studies about the steady state of the quantum skyrmion Hall effect, looking for eventual quantum skyrmion edge channels and their transport properties.

DOI: 10.1103/PhysRevResearch.5.033180

## I. INTRODUCTION

From fundamental physical processes to application-oriented information storage and processing, the stability of a physical effect is paramount. Some physical effects, especially quantum Hall effects, accommodate observables that are topologically protected, i.e., they are robust against a continuous deformation of selected parameters. Recently, experimental and theoretical studies have found topologically protected classical magnetic structures in thin films or effectively two-dimensional systems, which have been coined magnetic skyrmions [1–5], connected to earlier ideas in particle physics [6]. The stability of these objects and the possibility of creating them by electrical currents or time-controlled magnetic boundary conditions [7–10] promote the idea of using them in spintronics and as information carriers [11–13]. Furthermore, in sight of the ongoing miniaturization of magnetic skyrmions, they have also been proposed as ingredients in quantum computing [14].

Classical magnetic skyrmions experience an additional drag transversal to the direction of an applied electric current, which leads to an accumulation of skyrmions at one side [15–23]. The angle between the direction of motion and the direction of the current is called the Magnus angle of the skyrmion Hall effect. The question arises if there is a quantum version of the skyrmion Hall effect and, if so, which characteristics of the electronic Hall effects transfer, including hypothetical skyrmion edge channels with their quantized conductance. A previous study treating the quantum skyrmion as a product state and calculating an effective action for the quantum skyrmion demonstrated the existence of the Magnus force [24]. Yet the challenge in describing general quantum skyrmions comes with the large Hilbert spaces that need to be considered in two-dimensional spin systems carrying quantum skyrmions of a size of minimally $3 \times 3$ spins [25–27], which demand special theoretical techniques like density matrix renormalization group [28] or artificial neural networks [29] to investigate them numerically.

Another method to analyze quantum skyrmions is the use of localized spins from interacting electrons, like $f$ electrons to represent the skyrmions in a correlated electronic system [30]. Representing the skyrmions as electronic degrees of freedom has the advantage that we can treat considerably large quantum spin systems with established advanced numerical techniques for correlated electronic systems and that we can apply an electric current within the model without further assumptions. Interestingly, skyrmions in $f$-electron systems have been experimentally detected in $EuAl_4$, in which the skyrmions have been treated classically [31]. Yet the quantum nature of skyrmions in strongly correlated electronic systems is not well studied. Ultimately, a quantum skyrmion Hall effect could have direct practical applications extenting the manifold of suggested technical applications of magnetic skyrmions [32] to the quantum world. Moreover, fundamental questions about the topological nature of quantum skyrmions,

*Corresponding author: peters.robert.7n@kyoto-u.ac.jp

†Corresponding author: thore.posske@uni-hamburg.de

which, strictly speaking, gets lost because of quantum spin slip processes [27,33–35], could be answered when quantum skyrmions are connected to quantum Hall effects and their unambiguous topological origin.

In this paper, we numerically study a square lattice of localized $f$ electrons that are coupled to two-dimensional itinerant conduction ($c$) electrons in the presence of spin-orbit coupling and a small magnetic field perpendicular to the two-dimensional plane. Using dynamical mean-field theory, we reliably identify regions in parameter space that host quantum nanoskyrmions. We subsequently study the effect of a current in the itinerant electrons on the quantum skyrmion in linear response theory and find a strong initial drag into the direction perpendicular to the current, marking the onset of the quantum skyrmion Hall effect. The shift of the skyrmion is accompanied by an Edelstein effect and a magnetoelectric effect [36–42], which leads to a rotation of the localized $f$-electron spins. Our study stimulates further investigation of the quantum skyrmion Hall effect, especially its steady state, and possibly quantized skyrmion edge channels.

The remainder of this paper is structured as follows: In Sec. II, we introduce the model and the method. In Sec. III, we analyze the stability and structure of the quantum skyrmions for different model parameters. This is followed by Sec. IV, where we demonstrate the onset of the skyrmion Hall effect using linear response theory. Finally, in Sec. V, we discuss our results and conclude the paper.

## II. MODEL AND METHOD

Motivated by the discovery of magnetic skyrmions in Eu compounds [31], including partially filled $f$ electrons, we focus here on magnetically ordered ground states and low-energy metastable states in $f$-electron systems on a square lattice with a lattice constant of $a$ on the order of half a nanometer. In particular, we study the ground states of a noncentrosymmetric $f$-electron system described by a periodic Anderson model [41,43,44]. It is important to note that we explicitly start with an electronic Hamiltonian instead of a quantum spin model. Thus, charge fluctuations and other effective interactions besides the effective Heisenberg and Dzyaloshinskii–Moriya (DM) interaction generally affect the ground state. Furthermore, due to the hybridization between the itinerant conduction ($c$) electrons and the $f$ electrons, the magnetic moments generated by the $f$ electrons are intrinsically coupled to the $c$ electrons. Such a coupling, which is necessary to observe skyrmion Hall and skyrmion drag effects, does hence not need to be inserted manually but is naturally included.

Our model Hamiltonian can be split into a single-particle part, $H_0$, and an interaction part, $H_U$. The single-particle Hamiltonian is

$$\begin{aligned} H_0(\boldsymbol{k}) = {} & (t[\cos(k_x)+\cos(k_y)] + [\mu_c+\mu_f]/2)\boldsymbol{c}_{\boldsymbol{k}}^{\dagger}\boldsymbol{c}_{\boldsymbol{k}} \\ & + (t[\cos(k_x)+\cos(k_y)] + [\mu_c-\mu_f]/2)\boldsymbol{c}_{\boldsymbol{k}}^{\dagger}\sigma^0\tau^z\boldsymbol{c}_{\boldsymbol{k}} \\ & - 2\alpha_c \sin(k_y)\boldsymbol{c}_{\boldsymbol{k}}^{\dagger}\sigma^x\tau^x\boldsymbol{c}_{\boldsymbol{k}} + 2\alpha_c \sin(k_x)\boldsymbol{c}_{\boldsymbol{k}}^{\dagger}\sigma^y\tau^x\boldsymbol{c}_{\boldsymbol{k}} \\ & + V\boldsymbol{c}_{\boldsymbol{k}}^{\dagger}\sigma^0\tau^x\boldsymbol{c}_{\boldsymbol{k}} + B\boldsymbol{c}_{\boldsymbol{k},\rho_1\tau_1}^{\dagger}\sigma^z\tau^0\boldsymbol{c}_{\boldsymbol{k}}, \end{aligned} \tag{1}$$

where $\boldsymbol{c}_{\boldsymbol{k}} = (c_{k_x,k_y,\uparrow}, f_{k_x,k_y,\uparrow}, c_{k_x,k_y,\downarrow}, f_{k_x,k_y,\downarrow})$ is the spinor containing the momentum space annihilation operators of the itinerant electrons and $f$ electrons, respectively, corresponding to the real-space operators $c_{i,j,\sigma}$ and $f_{i,j,\sigma}$ at site $(i,j)$ of a square lattice with spin $\sigma$. The matrices $\sigma^{\lambda} = s^{\lambda}\otimes s^0$ and $\tau = s^0\otimes s^{\lambda}$ denote the Pauli matrices on the spin and sublattice space, respectively, where $s$ are the bare Pauli matrices. The particle number operators are $n^c_{i,j,\sigma} = c^{\dagger}_{i,j,\sigma}c_{i,j,\sigma}$ and $n^f_{i,j,\sigma} = f^{\dagger}_{i,j,\sigma}f_{i,j,\sigma}$. The strength of the nearest neighbor hopping of the $c$ electrons on the square lattice is denoted by $t$. Throughout this paper, we use $t$ as the unit of energy. $\mu_c$ and $\mu_f$ are local energies of the $c$ and $f$ electrons, respectively. $V$ is a local hybridization between the $c$ and $f$ electrons as commonly used in the periodic Anderson model. $B$ corresponds to a small magnetic field applied in the $z$ direction. Finally, we include a spin-orbit coupling between the $c$ and $f$ electrons with hopping amplitude $\alpha_c$. This spin-orbit coupling corresponds to a Rashba-type spin-orbit interaction as present in noncentrosymmetric $f$-electron systems [43]. The interaction part of the Hamiltonian is

$$H_U = U\sum_{i,j} n^f_{i,j,\uparrow}n^f_{i,j,\downarrow}, \tag{2}$$

corresponding to a density-density interaction between $f$ electrons on the same lattice site. The full Hamiltonian is

$$H = H_0 + H_U. \tag{3}$$

The calculations are performed on a finite lattice $L_x \times L_y = 11 \times 11$ with periodic boundary conditions.

To find the ground state of this quantum model, we use the real-space dynamical mean-field theory (RDMFT) [45–49]. RDMFT maps each atom of a unit cell (finite lattice) on its own quantum impurity model by calculating the local Green's function

$$G_{n,m}(z) = [z - \tilde{h}_0 - \Sigma(z)]^{-1}_{n,m}, \tag{4}$$

where $\tilde{h}_0$ is the single-particle matrix of the Fourier transform of $H_0$ in Eq. (1) into real space, i.e., $\tilde{H}_0 = \sum_{n,m} c^{\dagger}_n \tilde{h}_{n,m} c_m$. Here $n$ and $m$ are super indices including the lattice positions, the $f$-$c$ sublattice, and the spin. Furthermore, $\Sigma(z)$ is a matrix including the local self-energies of each lattice site in the finite lattice, where, by the defining approximation of RDMFT, $\Sigma_{n,m}(z)$ vanishes when the spatial components of $n$ and $m$ differ. Writing the local Green's function as

$$G_{n,m} = [z - \Delta_{n,m}(z) - \Sigma_{n,m}(z)]^{-1}, \tag{5}$$

we can map each lattice site on a quantum impurity model, where $\Delta_{n,m}(z)$ is the local hybridization of the impurity model. This hybridization function describes the environment for one lattice site created by the rest of the lattice. Here the self-energy differs for each lattice site, and hence this hybridization function is different for each lattice site. Summarizing the numerical procedure, the local hybridization functions define quantum impurity models, which are solved to obtain the local self-energy for each lattice site. These updated self-energies are then used in Eq. (4), which defines a self-consistency problem. To calculate the self-energy of each lattice site, we use the numerical renormalization group

[50–52], which can calculate accurate Green's functions and self-energies at low temperatures.

The magnetic properties of the periodic Anderson model without Rashba spin-orbit interaction are well understood within the DMFT approximation [45]. At half-filling, $\langle n^c_{i,j}\rangle = \langle n^f_{i,j}\rangle = 1$, on a square lattice, the periodic Anderson model orders antiferromagnetically for weak hybridization strengths $V$ [48]. For large hybridization strengths, the periodic Anderson model at half-filling becomes a Kondo insulator. On the other hand, when the number of $c$ electrons is small and the $f$ electrons are nearly half-filled, the system orders ferromagnetically [53]. This paper aims to study the existence and properties of magnetic skyrmions in a ferromagnetic periodic Anderson model, including Rashba spin-orbit interaction. We thus look for parameters where the $f$ electrons are nearly half-filled, and the $c$-electron filling is about $\langle n^c\rangle \approx 0.2$.

An exhaustive search of the parameter space of the periodic Anderson model for stable quantum skyrmions in the ground state is numerically unfeasible. In advance to our fully quantum-mechanical calculations, we therefore first identify candidate parameter regions where the ground state or low-energy metastable states accommodate magnetic skyrmions. We do so by mapping Eq. (1) to a classical Heisenberg spin model with nearest-neighbor coupling by integrating out the $c$ electrons using second-order perturbation theory, which obtains the RKKY spin-spin interactions [54–56]. We then use classical Monte Carlo methods to find the ground states of these spin models [57]. In particular, we have varied in this procedure the local hybridization $V$, the spin-orbit coupling $\alpha_c$, and the $c$-electron level position, $\mu_c$. We subsequently transfer parameter configurations where we find a classical skyrmion to the quantum model and conduct RDMFT calculations to obtain the system's ground state. Here the presence of magnetic skyrmions in the corresponding classical model generally is a good indicator for quantum skyrmions in the quantum model. Setting $U/t = 6$ and $\mu_f/t = -3$, corresponding to half-filling of the $f$ electrons, we find quantum skyrmions in a ferromagnetic background for $V = t$, $\mu_c/t \approx 3.6$, and a finite spin-orbit coupling in combination with a magnetic field, in agreement with previous results on classical and quantum magnetic skyrmions [25–28]. In the RDMFT calculations, we vary the strength of the spin-orbit interaction, $\alpha_c$, and the strength of the magnetic field, $B$, in the region according to the results of the classical calculations.

## III. STRUCTURE AND STABILITY OF MAGNETIC SKYRMIONS IN THE PERIODIC ANDERSON MODEL

To unambiguously identify a magnetic skyrmion, we break the spin translation symmetry of the model in the first DMFT iteration. By this, we select a specific state of the translationally invariant space of ground states. We use two different strategies in our calculations. We either start with a ferromagnetic solution where all $f$ electrons point downwards and flip a single $f$ electron upwards. Alternatively, we directly start with a magnetic skyrmion solution obtained for a different set of parameters. Then, by iterating the DMFT self-consistency equation, we find possible, stable magnetic skyrmion solutions when the algorithm converges. In the skyrmion phase, both initial states lead to identical DMFT solutions. We show the convergence of the self-energies for a typical skyrmion solution in Appendix B.

To verify the existence of a magnetic skyrmion, we calculate the spin expectation values of the $c$ and $f$ electrons for each lattice site,

$$\boldsymbol{S}^c_{\boldsymbol{r}} = \langle c^\dagger_{\boldsymbol{r},\rho_1}\boldsymbol{\sigma}_{\rho_1,\rho_2}c_{\boldsymbol{r},\rho_2}\rangle, \tag{6}$$

$$\boldsymbol{S}^f_{\boldsymbol{r}} = \langle f^\dagger_{\boldsymbol{r},\rho_1}\boldsymbol{\sigma}_{\rho_1,\rho_2}f_{\boldsymbol{r},\rho_2}\rangle, \tag{7}$$

where $\boldsymbol{r} = (i, j)$ corresponds to the coordinates of a lattice site and $\boldsymbol{\sigma} = (\sigma^x, \sigma^y, \sigma^z)$ is the vector containing the spin space Pauli matrices. Using these spin expectation values, we calculate the local lattice skyrmion density for the $f$ and $c$ electrons based on the solid angle spanned by three vectors as

$$N^d_{\boldsymbol{r}_1,\boldsymbol{r}_2,\boldsymbol{r}_3} = \frac{1}{2\pi}\tan^{-1}\left[\frac{\boldsymbol{S}^d_{\boldsymbol{r}_1}\cdot\left(\boldsymbol{S}^d_{\boldsymbol{r}_2}\times\boldsymbol{S}^d_{\boldsymbol{r}_3}\right)}{\left(\frac{\hbar}{2}\right)^3 + \frac{\hbar}{2}\left(\boldsymbol{S}^d_{\boldsymbol{r}_1}\boldsymbol{S}^d_{\boldsymbol{r}_2} + \boldsymbol{S}^d_{\boldsymbol{r}_1}\boldsymbol{S}^d_{\boldsymbol{r}_3} + \boldsymbol{S}^d_{\boldsymbol{r}_2}\boldsymbol{S}^d_{\boldsymbol{r}_3}\right)}\right], \tag{8}$$

where $d$ either stands for $f$ or $c$ electrons, $\boldsymbol{r}_1$, $\boldsymbol{r}_2$, and $\boldsymbol{r}_3$ are nearest-neighbor lattice sites spanning an elemental triangle $\langle \boldsymbol{r}_1, \boldsymbol{r}_2, \boldsymbol{r}_3\rangle$ in the densest triangular tessellation of the lattice. The sum of this skyrmion density over all triangles spanning the square lattice yields the skyrmion number

$$N^{c/f} = \sum_{\langle \boldsymbol{r}_1,\boldsymbol{r}_2,\boldsymbol{r}_3\rangle} N^{c/f}_{\boldsymbol{r}_1,\boldsymbol{r}_2,\boldsymbol{r}_3}. \tag{9}$$

Unlike in a classical calculation, the spin expectation values in a quantum model do not need to be $\hbar/2$ in magnitude. In fact, these expectation values are usually smaller due to quantum fluctuations, $|\boldsymbol{S}| < \hbar/2$. We thus calculate two types of skyrmion densities: One is the quantum skyrmion density/number using un-normalized spin expectation values. The second type is a classical skyrmion density, where we normalize all spin expectation values to $\hbar/2$ before using them in Eq. (8). The skyrmion number is an integer when using normalized spin expectation values. When using un-normalized spin expectation values, the skyrmion number is not quantized, and instead its magnitude is an indicator of the skyrmion stability [27], similarly to the scalar chirality defined in Ref. [25].

A representative magnetic skyrmion solution is shown in Fig. 1 calculated for a spin-orbit coupling $\alpha_c/t = 0.3$ and a magnetic field $B/t = 0.002$. We note that within the accuracy of our calculations, we cannot find discernible energy differences between the ferromagnetic configuration and the magnetic skyrmion. The described skyrmions can, therefore, be metastable excitations on a ferromagnetic background with almost vanishing excitation energy or present in the ground state itself. Such an almost degenerate situation is favorable for applications in racetrack devices. If skyrmions were energetically strongly favorable, then a skyrmion lattice would form instead of individual skyrmions. Figure 1 shows the spin texture of the $f$ and $c$ electrons underlaid with the local skyrmion density for normalized spin expectation values as two-dimensional color plot, see Eq. (8). Due to the local hybridization, $V$, which leads to an effective antiferromagnetic interaction between the $c$ and $f$ electrons, the spins of the $c$ and $f$ electrons mostly point in opposite directions, with

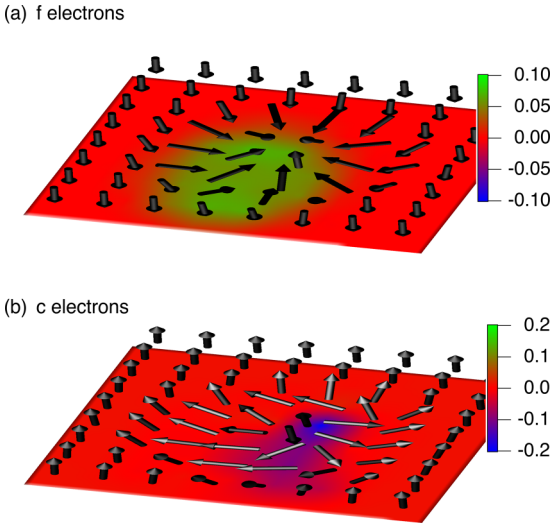


FIG. 1. Magnetic skyrmion in an $f$ electron system. A skyrmion forms in the $f$ electrons, depicted by their spin expectation values (a). The color code corresponds to the local skyrmion density in Eq. (8). As a result, an antiskyrmion forms in the itinerant $c$ electrons (b). The antiskyrmion is considerably less polarized, $|\langle S^c\rangle|_a \approx 0.03\frac{\hbar}{2}$. The spin expectation values are shown normalized for better visualization. Parameters: spin-orbit coupling $\alpha_c/t = 0.3$ and magnetic field $B/t = 0.002$.

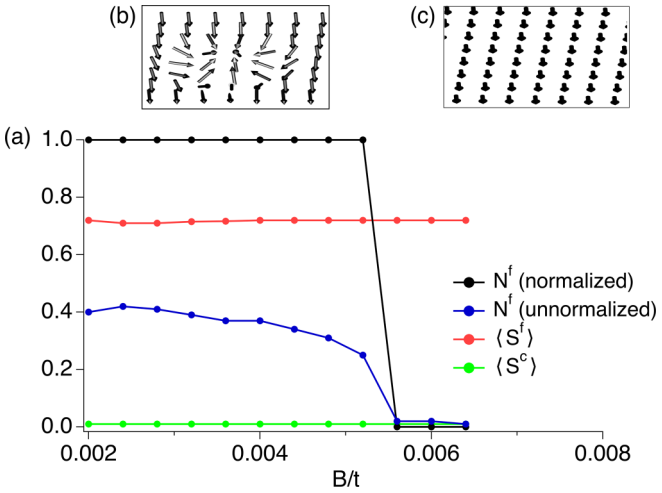


FIG. 2. Magnetic field dependence of magnetic skyrmions for spin-orbit coupling $\alpha_c = 0.3t$. Panel (a) shows the normalized and un-normalized skyrmion number and average spin expectation values of the $c$ and $f$ electrons. The skyrmion number drops to zero at $B/t \approx 0.0056$, and the spins align ferromagnetically, consistent with studies on quantum skyrmions in spin lattices [25,28]. The average spin expectation value $|\langle S^{f/c}\rangle|_a$ of the $c$ and $f$ electrons alone does not indicate this phase transition. Panels (b) and (c) show typical $f$-spin configurations for small (skyrmionic configuration at $B/t = 0.002$) and large magnetic fields (ferromagnetic configuration at $B/t = 0.006$), respectively.

deviations in the skyrmion's center, where the Rashba interaction and the itinerant character of the $c$ electrons play a stronger role. The combined state corresponds to a bound skyrmion-antiskyrmion pair where the $f$ electrons form a magnetic skyrmion with skyrmion number $N^f = 1$ and the $c$ electrons form a magnetic antiskyrmion with skyrmion number $N^c = -1$. However, in this system, the spin expectation values of the $c$ and $f$ electrons are of very distinct origins and magnitudes. Because the $f$ electrons are strongly interacting, they form localized magnetic moments, and their spin expectation values in this calculation are approximate $|\langle S^f\rangle|_a \approx 0.75\frac{\hbar}{2}$. They are not perfectly polarized due to the entanglement between the $c$ and the $f$ electrons. On the other hand, the $c$ electrons are noninteracting, and their spin expectation values vary around $|\langle S^c\rangle|_a \approx 0.03\frac{\hbar}{2}$. The $c$ electrons' polarization is a direct cause of the hybridization with the magnetized $f$ electrons and, thus, a secondary effect. In this situation, the skyrmion of the $f$ electrons and the antiskyrmion of the $c$ electrons do not annihilate. This is revealed by the finite total skyrmion number calculated with un-normalized spin expectation values. This is indeed different from classical skyrmions, where the magnitude of the spin vectors is normalized. The reduced polarization decreases the topological protection of the magnetic skyrmion. The smaller the spin expectation value, the easier the spin can be flipped, and the magnetic skyrmion is destroyed [27]. On the other hand, this facilitates manipulating them as necessary for technical applications.

Next, we analyze the stability of the magnetic skyrmion for different magnetic field strengths, as shown in Fig. 2. As stated above, we generally apply a small magnetic field which helps to stabilize the magnetic skyrmion against spin spiral solutions [25,28]. In Fig. 2(a), we show the skyrmion number using normalized and un-normalized spins, respectively. We observe that, while the skyrmion number (normalized) is constantly one for $B/t \lesssim 0.0056 = B_c$, the skyrmion number using un-normalized spin expectation values is $N^f \approx 0.4$ and gradually drops for an increased magnetic field until $B_c$ is reached. The difference between these numbers demonstrates the relevance of quantum effects to the system at hand. We furthermore show the average spin expectation values of the $c$ and $f$ electrons, indicating that the $f$ electrons are considerably more stronger polarized than the $c$ electrons. Furthermore, for magnetic fields stronger than $B_c$, we only find ferromagnetic solutions. Figures 2(b) and 2(c) give representative spin textures of the $f$ electrons for the corresponding parameter regimes, i.e., small and large magnetic fields.

We next analyze the structure of the skyrmion depending on the strength of the Rashba spin-orbit coupling $\alpha_c$. We show the skyrmion number using normalized spin expectation values, the skyrmion number using un-normalized spin expectation values, and the average spin expectation values ($\langle S^f\rangle$ and $\langle S^c\rangle$) in Fig. 3(a). Increasing the Rashba interaction, the $f$-electron spin expectation value is slightly suppressed, while the $c$-electron spin expectation value slightly increases. This increase in the $c$ electron magnetization can be explained by the stronger coupling between the $c$ and $f$ electrons. While we need $\alpha_c/t > 0$ to create a finite DM interaction that stabilizes the magnetic skyrmion, we see that for increasing $\alpha_c$ the skyrmion gets destabilized and for $\alpha_c/t > 0.4$, magnetic skyrmions become unstable indicated by the vanishing skyrmion number. To analyze this transition further, we calculate the average size of the skyrmion. First, the center of the

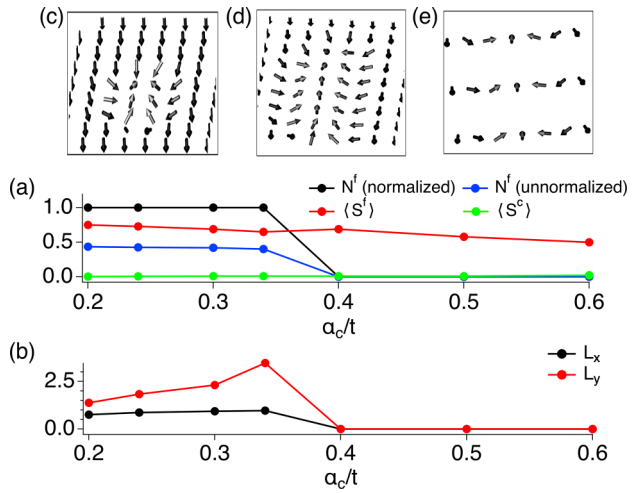


FIG. 3. Dependence of magnetic skyrmions on the spin-orbit coupling for $B/t = 0.002$. Panel (a) shows the skyrmion number (normalized), skyrmion number (un-normalized), and averaged spin expectation values ($c$ and $f$ electrons), $\langle \boldsymbol{S}^f \rangle_a$ and $\langle \boldsymbol{S}^c \rangle_a$, for different strengths of the Rashba interaction. The skyrmion changes to a spin density wave at $\alpha_c/t = 0.4$. Panel (b) shows the extension of the skyrmion in the $x$ and $y$ direction; see Eq. (11). Panels (c)–(e) show representative spin configurations for small ($\alpha_c = 0.2t$), medium ($\alpha_c = 0.35t$), and large ($\alpha_c = 0.5t$) spin-orbit interaction.

skyrmion created by the $f$ electrons is

$$\boldsymbol{R}_S = \sum_{\langle \boldsymbol{r}_1, \boldsymbol{r}_2, \boldsymbol{r}_3 \rangle} N^f_{\boldsymbol{r}_1, \boldsymbol{r}_2, \boldsymbol{r}_3} \frac{\boldsymbol{r}_1 + \boldsymbol{r}_2 + \boldsymbol{r}_3}{3}, \tag{10}$$

where $\boldsymbol{r}_1$, $\boldsymbol{r}_2$, and $\boldsymbol{r}_3$ are the coordinates of the lattice sites spanning the elemental triangle as explained below Eq. (8). The extension of the skyrmion in the $x$ and the $y$ directions $\boldsymbol{L} = (L_x, L_y)$ is then given as

$$\boldsymbol{L}_x^2 = \sum_{\boldsymbol{r}_1, \boldsymbol{r}_2, \boldsymbol{r}_3} N^f_{\boldsymbol{r}_1, \boldsymbol{r}_2, \boldsymbol{r}_3} \left( \frac{\boldsymbol{x}_1 + \boldsymbol{x}_2 + \boldsymbol{x}_3}{3} - \boldsymbol{x}_S \right)^2, \tag{11}$$

$$\boldsymbol{L}_y^2 = \sum_{\boldsymbol{r}_1, \boldsymbol{r}_2, \boldsymbol{r}_3} N^f_{\boldsymbol{r}_1, \boldsymbol{r}_2, \boldsymbol{r}_3} \left( \frac{\boldsymbol{y}_1 + \boldsymbol{y}_2 + \boldsymbol{y}_3}{3} - \boldsymbol{y}_S \right)^2, \tag{12}$$

where $x_i$ ($y_i$) is the $x$ ($y$) component of the position $\boldsymbol{r}_i$ and the center of the skyrmion is $\boldsymbol{R}_s = (x_s, y_s)$. In Fig. 3(b), we show the extension of the skyrmion in the $x$ and $y$ directions depending on the Rashba spin-orbit interaction. We see that while the average extension of the skyrmion in the $x$ direction remains unchanged when increasing $\alpha_c$, the magnetic skyrmion is strongly elongated in the $y$ direction. At $\alpha_c/t \approx 0.4$, the magnetic skyrmion changes into a spiral phase, again consistent with findings for quantum skyrmions on nonelectronic spin lattices [25,28]. Representative spin textures of the $f$ electrons are shown in Figs. 3(c)–3(e), depicting a skyrmion for small $\alpha_c$ [Fig. 3(c)], an elongated skyrmion close to the phase transition [Fig. 3(d)], and a spiral wave for large $\alpha_c$ [Fig. 3(e)]. For larger values of the spin-orbit coupling, we do not find stable skyrmion solutions.

Finally, we note that we have confirmed the stability of the quantum skyrmion phase for smaller lattice sizes, such as $7\times7$. Magnetic skyrmions remain stable as long as their elongation is smaller than the lattice width. Furthermore, we do not find an even/odd effect in the lattice width, which can be understood by the fact that all spins are ferromagnetically aligned far away from the magnetic skyrmion, irrespective of changes of the lattice sizes once it exceeds the size of the quantum skyrmion.

## IV. CHARGE-DRIVEN QUANTUM SKYRMIONS—THE ONSET OF THE QUANTUM SKYRMION HALL EFFECT

Finally, we study the response of the identified stable skyrmion textures to an applied charge current in the itinerant $c$ electrons. To do this, we calculate the change in the spin expectation values of all lattice sites in linear response theory. We focus on describing the time-transient behavior of the system. A description of the nonequilibrium steady state poses considerable numerical challenges, as discussed in the concluding remarks.

In linear response, the change in an expectation value of operator $A$ resulting from a perturbation $B$ is given by

$$\langle A \rangle(\tau) = \langle A \rangle(0) + \int_0^\tau d\tau' X_{AB}(\tau - \tau'), \tag{13}$$

$$X_{AB}(\tau - \tau') = i\Theta(\tau - \tau')\langle [A(\tau), B(\tau')] \rangle, \tag{14}$$

where $\Theta(\tau)$ is the Heaviside step function. Because we are interested in the linear response of the spin expectation values of the $f$ electrons to a charge current in the itinerant electrons, we use

$$A = f^\dagger_{\boldsymbol{r},\rho_1} \sigma^{x/y/z}_{\rho_1\rho_2} f_{\boldsymbol{r},\rho 2} = S^{x/y/z}, \tag{15}$$

$$B = J^c = -iJ \sum_{i,j,\sigma} (c^\dagger_{i+1,j,\sigma} c_{i,j,\sigma} - c^\dagger_{i-1,j,\sigma} c_{i,j,\sigma}), \tag{16}$$

where $A$ corresponds exactly to the local spin of an $f$ electron and $B$ is the charge current operator in the $c$ electrons. For these operators, Eq. (14) corresponds to a nonlocal two-particle Green's function. Using the DMFT approximation, where vertex corrections in nonlocal Green's functions vanish, we write these two-particle Green's functions as the convolution of two single-particle Green's functions. Then, we calculate the time evolution of the spin expectation values of all spins. Because the self-energy depends on the lattice site, also the time evolution of the spin expectation value depends on the lattice site. This is shown in Fig. 4, where we show the change of the $x$, $y$, and $z$ component of the spin expectation values $\Delta\langle S^x \rangle(\tau)$, $\Delta\langle S^y \rangle(\tau)$, and $\Delta\langle S^z \rangle(\tau)$ along the $x$ direction of the lattice across the center of the skyrmion solution for $\alpha_c/t = 0.3$ (shown in Fig. 1). Specifically, the spin expectation values are shown for lattice sites $(x_S + x, y_S)$, where $\boldsymbol{R}_S = (x_S, y_S)$ is the center of the skyrmion, see Eq. (10). $\Delta\langle S_x \rangle$ and $\Delta\langle S_z \rangle$ show a strong dependence on the position close to the center of the skyrmion. $\Delta\langle S_z \rangle$ changes even its sign when changing the position from the left of the center to the right of the center. On the other hand, $\Delta\langle S_y \rangle$ is nearly independent of the lattice site. Also, while $\Delta\langle S_z \rangle$ becomes small for spins far away from the skyrmion center, $\Delta\langle S_x \rangle$ and $\Delta\langle S_y \rangle$ are nonzero. Thus, even in the ferromagnetic region away from the skyrmion center, $\langle S_x \rangle$ and $\langle S_y \rangle$ change.

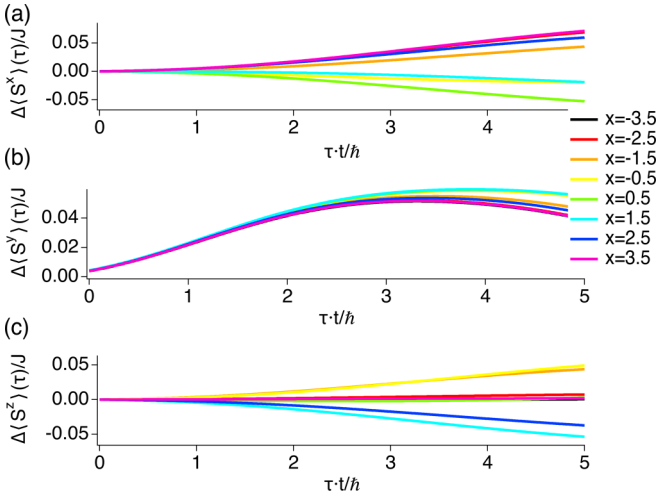


FIG. 4. Time-resolved change of the spin expectation values $\Delta\langle S^x\rangle(\tau)$ (a), $\Delta\langle S^y\rangle(\tau)$ (b), and $\Delta\langle S^z\rangle(\tau)$ (c) scanned in the $x$ direction across the center of the magnetic skyrmion at lattice sites $(x_S + x, y_S)$, calculated by linear response theory for $\alpha_c/t = 0.3$. Here $\boldsymbol{R}_S = (x_S, y_S)$ is the center of the skyrmion, see Eq. (10). The change of the spin expectation values is normalized by the strength of the current, $J$. The expectation values start oscillating when the validity regime of the linear response theory is left.

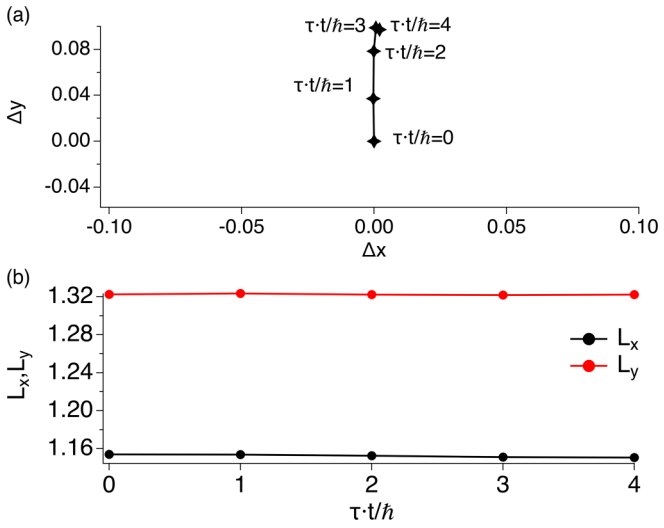


FIG. 6. Onset of the quantum skyrmion Hall effect for $\alpha_c/t = 0.3$ and $B/t = 0.002$: Shown are the center (a) and the size (b) of the quantum magnetic skyrmion depending on time, calculated by linear response theory. The quantum skyrmion starts moving almost perpendicularly to the applied current, indicating a Magnus angle close to 90°. When the validity of the linear response calculations is left, the skyrmion slows down. The size of the skyrmion stays constant over time, indicating a negligible smearing of the structure compared to its motion.

This rotation of the spin in the ferromagnetic state when a charge current is applied is explained by the Edelstein and the magnetoelectric effect [41]; in a system where the Fermi surface is split due to the Rashba spin-orbit coupling, a charge current results in an accumulation of spin. This can be seen here as a rotation of the spin expectation values in the $x$ and the $y$ direction, even far away from the magnetic skyrmion. Furthermore, we emphasize that the linear-response results only remain valid within sufficiently small times $\tau$. In Fig. 4, we see that the initial linear trend in $\tau$ is reduced, and, as an expected artifact from linear response theory, all spin expectation values start oscillating after a certain individual time. The change of all spin expectation values for $\tau \cdot t/\hbar = 2$ and $\tau \cdot t/\hbar = 4$ are visualized in Fig. 5 as arrows. Each arrow corresponds to the direction of the local change in the spin expectation values $\Delta\langle \boldsymbol{S}\rangle(\tau)$. The actual length of each change is

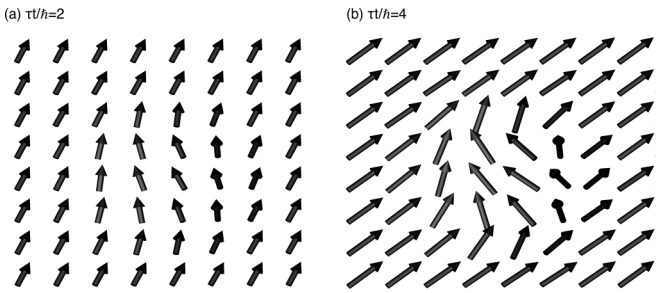


FIG. 5. Changes in the spin expectation values at (a) $\tau \cdot t/\hbar = 2$ and (b) $\tau \cdot t/\hbar = 4$ for $\alpha_c/t = 0.3$. The length of the vectors has been multiplied by five in both figures to enhance visibility. The actual magnitude of the changes are (a) $|\Delta\langle \boldsymbol{S}\rangle(\tau)| \approx 0.04\frac{\hbar}{2}J$ and (b) $|\Delta\langle \boldsymbol{S}\rangle(\tau)| \approx 0.07\frac{\hbar}{2}J$.

$|\Delta\langle \boldsymbol{S}\rangle(\tau)| \approx 0.04\frac{\hbar}{2}J$ and $|\Delta\langle \boldsymbol{S}\rangle(\tau)| \approx 0.07\frac{\hbar}{2}J$ for $\tau \cdot t/\hbar = 2$ and $\tau \cdot t/\hbar = 4$, respectively. We see that in the ferromagnetic region, all spins are rotated in the same direction. Only close to the magnetic skyrmion, the change in the spin expectation values significantly depends on the lattice site.

Finally, we take the time evolution of each spin on the lattice and calculate the skyrmion density and the time-dependent size and position of the skyrmion according to Eqs. (10) and (11). By Eq. (14), we find that the center of the skyrmion moves almost perpendicularly to the applied current, as shown in Fig. 6(a). While the current is applied in the $x$ direction, the skyrmion moves in the positive $y$ direction. Thus, our results demonstrate the onset of a quantum skyrmion Hall effect with a Magnus angle close to 90°. Notably, the size of the skyrmion effectively remains constant during the motion, shown in Fig. 6(b).

## V. DISCUSSION

In conclusion, we show that noncentrosymmetric $f$-electron systems with spin-orbit coupling in the presence of a small external magnetic field can host quantum nanoskyrmions in the ground state, and we demonstrate the onset of the quantum skyrmion Hall effect when applying a charge current, which is accompanied by an Edelstein and magnetoelectric effect.

The reason for the stability of the quantum skyrmion is an effective DM interaction generated by the spin-orbit interaction and a local density-density interaction. Despite the itinerant $c$ electrons being magnetized like an antiskyrmion, the quantum skyrmions of the $f$ electrons remain stable and dominate the physical behavior of the system because of its

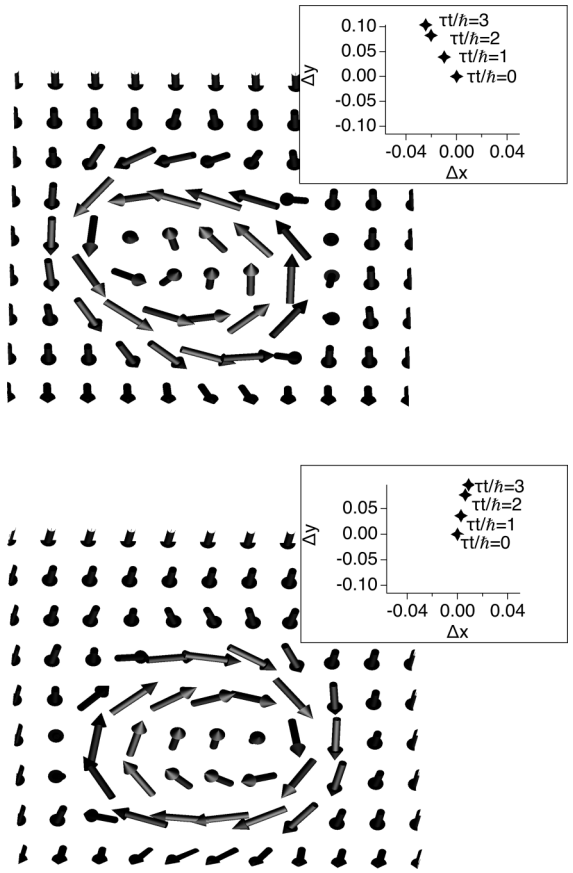


FIG. 7. Spin texture including a magnetic skyrmion for $\alpha_c/t = 0.3$ (top panel) and $\alpha_c/t = -0.3$ (bottom panel). The insets show the initial motion of the center of the skyrmion after a charge current in the $x$ direction is applied.

considerably stronger polarization due to strong correlations. Concerning the quantum skyrmion Hall effect, we observe a Magnus angle close to 90°. This is consistent with the behavior of classical skyrmions, where the Magnus angle increases when the size of the skyrmions is smaller or when dissipative effects are small [22,23]. Both is the case for the observed quantum nanoskyrmions. Furthermore, no quantum skyrmion pinning is visible in our study. We note that our method can only describe the onset of the skyrmion motion. In particular, in a full nonequilibrium calculation, time-dependent spin expectation values would lead to time-dependent self-energies. The system would adapt to the changed spin expectation values and backaction effects would alter our conclusions when the linear-response regime is left. For example, linear response theory can permanently decrease the polarization locally, ultimately resulting in a site with vanishing spin polarization. However, this situation is energetically unfavorable due to the strong density-density interaction. Thus, in a full nonequilibrium calculation, self-energies will change in a way that an atom with vanishing spin polarization is prevented, rendering the quantum magnetic skyrmion stable and letting it continue its motion perpendicular to an applied current. Yet a full nonequilibrium calculation, as well as a steady-state analysis, goes beyond the scope of the current paper and is left for future work.

We note that other forms of spin-orbit interaction also lead to stable quantum nanoskyrmions in the $f$-electron system at hand. We show the results for a different form of the spin-orbit interaction, where the momenta couple to the same spin direction, in Appendix A. Also in these systems, the spin-orbit interaction results in a spin accumulation when a current is applied, which leads to a site-dependent change of the spin expectation values, and to a skyrmion Hall effect. These results emphasize that the existence of magnetic skyrmions in strongly correlated $f$-electron systems with spin-orbit coupling and the skyrmion Hall effect is a general effect.

## ACKNOWLEDGMENTS

All authors acknowledge funding by the Kyoto University-Hamburg University (KU-UHH) international partnership funding program for 2021 and 2022. R.P. is supported by JSPS KAKENHI No. JP18K03511 and No. JP23K03300. Parts of the numerical simulations in this work have been done using the facilities of the Supercomputer Center at the Institute for Solid State Physics, the University of Tokyo. J.N.-S. acknowledges support by the Cluster of Excellence "CUI: Advanced Imaging of Matter" of the Deutsche Forschungsgemeinschaft (DFG) EXC 2056 Project ID 390715994 and the Universität Hamburg's Next Generation Partnership funded under the Excellence Strategy of the Federal Government and the Länder. T.P. acknowledges funding by the DFG (Project No. 420120155) and the European Union (ERC, QUANTWIST, Project No. 101039098). Views and opinions expressed are, however, those of the authors only and do not necessarily reflect those of the European Union or the European Research Council. Neither the European Union nor the granting authority can be held responsible for themxqry.

## APPENDIX A: DIFFERENT FORM OF SPIN-ORBIT INTERACTION

To demonstrate that our results are robust for different types of spin-orbit coupling, we repeat our analysis using a

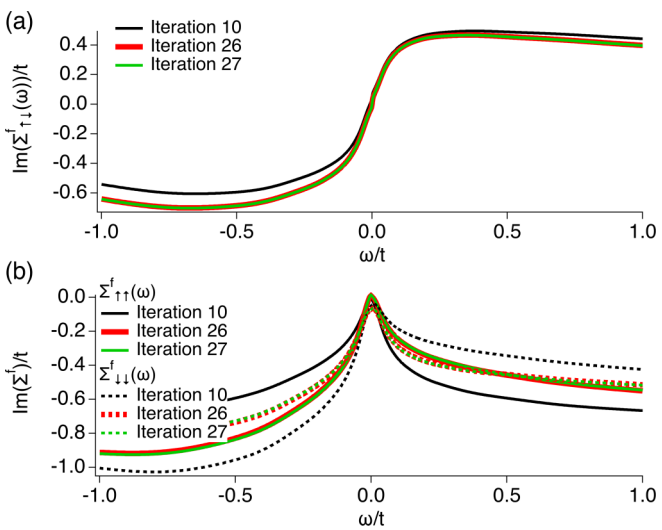


FIG. 8. Convergence of the diagonal and off-diagonal self-energies of the $f$ electrons for a lattice site left of the skyrmion center.

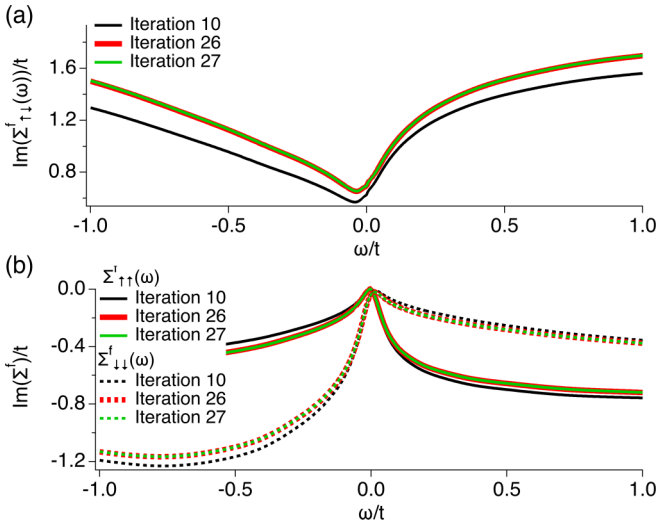


FIG. 9. Convergence of the diagonal and off-diagonal self-energies of the $f$ electrons for a lattice site below the skyrmion center.

spin-orbit interaction of the form

$$H_{\mathrm{SOI}}(\boldsymbol{k}) = 2\alpha_c(\sin(k_x)\boldsymbol{c}_{\boldsymbol{k}}^{\dagger}\sigma^x\tau^x\boldsymbol{c}_{\boldsymbol{k}} + \sin(k_y)\boldsymbol{c}_{\boldsymbol{k}}^{\dagger}\sigma^y\tau^x\boldsymbol{c}_{\boldsymbol{k}}). \tag{A1}$$

The rest of the Hamiltonian, including the two-particle interaction, is unchanged compared to the main text. In Fig. 7, we show two RDMFT solutions, including magnetic skyrmions, for $\alpha_c = \pm 0.3t$, where we again use a small magnetic field, $B/t = 0.002$, to stabilize the magnetic skyrmion [25–28]. The change in the sign of the spin-orbit interaction leads to a change in the rotation direction of the spin texture.

Furthermore, we apply a charge current in the $x$ direction for both solutions and find that the center of the quantum magnetic skyrmion dominantly moves into the positive $y$ direction. This is explained as follows: The change in the sign of the spin-orbit interaction leads not only to a reversal of the spin rotation inside the skyrmion but also changes the sign of the Edelstein and magnetoelectric effect. Thus, spins in these two examples are rotated in opposite directions when current is applied. As a result, both magnetic skyrmions move into the same, the positive $y$ direction.

## APPENDIX B: CONVERGENCE OF THE REAL-SPACE DMFT

In this Appendix, we demonstrate the convergence of the real-space DMFT in the magnetic skyrmion phase for $\alpha_c/t = 0.3$. In Figs. 8 and 9, we show representative self-energies of the $f$ electrons for two different lattice sites and different DMFT iterations. Panels (a) shows the off-diagonal self-energy, $\Sigma_{\uparrow\downarrow}(\omega)$, and panels (b) shows the diagonal self-energies, $\Sigma_{\uparrow\uparrow}(\omega)$ and $\Sigma_{\downarrow\downarrow}(\omega)$. On average, we need 20–30 DMFT iterations (depending on the parameters) to obtain a converged magnetic skyrmion solution. In both figures, we see that while the self-energy of the 10th iteration qualitatively shows the same behavior as iterations 26 and 27, quantitatively, it still differs from the converged self-energy. On the other hand, the self-energies of the 26th and 27th iterations lie on top of each other.


[1] A. Bogdanov, New localized solutions of the nonlinear field-equations, Pis'ma Zh. Éksp. Teor. Fiz. **62**, 231 (1995) [JETP Lett. **62**, 247 (1995)].

[2] A. Bogdanov and A. Hubert, The stability of vortex-like structures in uniaxial ferromagnets, J. Magn. Magn. Mater. **195**, 182 (1999).

[3] S. Mühlbauer, B. Binz, F. Jonietz, C. Pfleiderer, A. Rosch, A. Neubauer, R. Georgii, and P. Böni, Skyrmion lattice in a chiral magnet, Science **323**, 915 (2009).

[4] X. Z. Yu, Y. Onose, N. Kanazawa, J. H. Park, J. H. Han, Y. Matsui, N. Nagaosa, and Y. Tokura, Real-space observation of a two-dimensional skyrmion crystal, Nature (London) **465**, 901 (2010).

[5] S. Heinze, K. Von Bergmann, M. Menzel, J. Brede, A. Kubetzka, R. Wiesendanger, G. Bihlmayer, and S. Blügel, Spontaneous atomic-scale magnetic skyrmion lattice in two dimensions, Nat. Phys. **7**, 713 (2011).

[6] T. H. R. Skyrme, A unified field theory of mesons and baryons, Nucl. Phys. **31**, 556 (1962).

[7] K. Everschor-Sitte, M. Sitte, T. Valet, A. Abanov, and J. Sinova, Skyrmion production on demand by homogeneous dc currents, New J. Phys. **19**, 092001 (2017).

[8] M. Stier, W. Häusler, T. Posske, G. Gurski, and M. Thorwart, Skyrmion-Anti-Skyrmion Pair Creation by In-Plane Currents, Phys. Rev. Lett. **118**, 267203 (2017).

[9] A. F. Schäffer, P. Siegl, M. Stier, T. Posske, J. Berakdar, M. Thorwart, R. Wiesendanger, and E. Y. Vedmedenko, Rotating edge-field driven processing of chiral spin textures in racetrack devices, Sci. Rep. **10**, 20400 (2020).

[10] P. Siegl, M. Stier, A. F. Schäffer, E. Y. Vedmedenko, T. Posske, R. Wiesendanger, and M. Thorwart, Creating arbitrary sequences of mobile magnetic skyrmions and antiskyrmions, Phys. Rev. B **106**, 014421 (2022).

[11] S. S. P. Parkin, M. Hayashi, and L. Thomas, Magnetic domain-wall racetrack memory, Science **320**, 190 (2008).

[12] R. Tomasello, E. Martinez, R. Zivieri, L. Torres, M. Carpentieri, and G. Finocchio, A strategy for the design of skyrmion racetrack memories, Sci. Rep. **4**, 6784 (2014).

[13] A. Fert, N. Reyren, and V. Cros, Magnetic skyrmions: Advances in physics and potential applications, Nat. Rev. Mater. **2**, 17031 (2017).

[14] C. Psaroudaki and C. Panagopoulos, Skyrmion Qubits: A New Class of Quantum Logic Elements Based on Nanoscale Magnetization, Phys. Rev. Lett. **127**, 067201 (2021).

[15] A. A. Thiele, Steady-State Motion of Magnetic Domains, Phys. Rev. Lett. **30**, 230 (1973).

[16] K. Everschor, M. Garst, R. A. Duine, and A. Rosch, Current-induced rotational torques in the skyrmion lattice phase of chiral magnets, Phys. Rev. B **84**, 064401 (2011).

[17] K. Everschor, M. Garst, B. Binz, F. Jonietz, S. Mühlbauer, C. Pfleiderer, and A. Rosch, Rotating skyrmion lattices by spin torques and field or temperature gradients, Phys. Rev. B **86**, 054432 (2012).

[18] J. Iwasaki, M. Mochizuki, and N. Nagaosa, Universal current-velocity relation of skyrmion motion in chiral magnets, Nat. Commun. **4**, 1463 (2013).

[19] J. Iwasaki, M. Mochizuki, and N. Nagaosa, Current-induced skyrmion dynamics in constricted geometries, Nat. Nanotechnol. **8**, 742 (2013).

[20] J. Sampaio, V. Cros, S. Rohart, A. Thiaville, and A. Fert, Nucleation, stability and current-induced motion of isolated magnetic skyrmions in nanostructures, Nat. Nanotechnol. **8**, 839 (2013).

[21] K.-W. Moon, J. Yoon, C. Kim, J.-H. Sim, S. K. Kim, S.-G. Je, and C. Hwang, An alternative understanding of the skyrmion hall effect based on one-dimensional domain wall motion, Appl. Phys. Expr. **15**, 123001 (2022).

[22] W. Jiang, X. Zhang, G. Yu, W. Zhang, X. Wang, M. B. Jungfleisch, J. E. Pearson, X. Cheng, O. Heinonen, K. L. Wang, Y. Zhou, A. Hoffmann, and S. G. E. Te Velthuis, Direct observation of the skyrmion hall effect, Nat. Phys. **13**, 162 (2016).

[23] K. Litzius, I. Lemesh, B. Krüger, P. Bassirian, L. Caretta, K. Richter, F. Büttner, K. Sato, O. A. Tretiakov, J. Förster, R. M. Reeve, M. Weigand, I. Bykova, H. Stoll, G. Schütz, G. S. D. Beach, and M. Klaüi, Skyrmion hall effect revealed by direct time-resolved x-ray microscopy, Nat. Phys. **13**, 170 (2016).

[24] R. Takashima, H. Ishizuka, and L. Balents, Quantum skyrmions in two-dimensional chiral magnets, Phys. Rev. B **94**, 134415 (2016).

[25] O. M. Sotnikov, V. V. Mazurenko, J. Colbois, F. Mila, M. I. Katsnelson, and E. A. Stepanov, Probing the topology of the quantum analog of a classical skyrmion, Phys. Rev. B **103**, L060404 (2021).

[26] V. Lohani, C. Hickey, J. Masell, and A. Rosch, Quantum-skyrmions in Frustrated Ferromagnets, Phys. Rev. X **9**, 041063 (2019).

[27] P. Siegl, E. Y. Vedmedenko, M. Stier, M. Thorwart, and T. Posske, Controlled creation of quantum skyrmions, Phys. Rev. Res. **4**, 023111 (2022).

[28] A. Haller, S. Groenendijk, A. Habibi, A. Michels, and T. L. Schmidt, Quantum skyrmion lattices in heisenberg ferromagnets, Phys. Rev. Res. **4**, 043113 (2022).

[29] A. Joshi, R. Peters, and T. Posske, Ground state properties of quantum skyrmions described by neural network quantum states, Phys. Rev. B **108**, 094410 (2023).

[30] K. Kobayashi and S. Hayami, Skyrmion and vortex crystals in the hubbard model, Phys. Rev. B **106**, L140406 (2022).

[31] R. Takagi, N. Matsuyama, V. Ukleev, L. Yu, J. S. White, S. Francoual, J. R. L. Mardegan, S. Hayami, H. Saito, K. Kaneko, K. Ohishi, Y. Ōnuki, T.-h. Arima, Y. Tokura, T. Nakajima, and S. Seki, Square and rhombic lattices of magnetic skyrmions in a centrosymmetric binary compound, Nat. Commun. **13**, 1472 (2022).

[32] C. Back, V. Cros, H. Ebert, K. Everschor-Sitte, A. Fert, M. Garst, T. Ma, S. Mankovsky, T. L. Monchesky, M. Mostovoy, N. Nagaosa, S. S. P. Parkin, C. Pfleiderer, N. Reyren, A. Rosch, Y. Taguchi, Y. Tokura, K. von Bergmann, and J. Zang, The 2020 skyrmionics roadmap, J. Phys. D **53**, 363001 (2020).

[33] S. K. Kim and Y. Tserkovnyak, Topological Effects on Quantum Phase Slips in Superfluid Spin Transport, Phys. Rev. Lett. **116**, 127201 (2016).

[34] T. Posske and M. Thorwart, Winding Up Quantum Spin Helices: How Avoided Level Crossings Exile Classical Topological Protection, Phys. Rev. Lett. **122**, 097204 (2019).

[35] V. Vijayan, L. Chotorlishvili, A. Ernst, S. S. P. Parkin, M. I. Katsnelson, and S. K. Mishra, Topological dynamical quantum phase transition in a quantum skyrmion phase, Phys. Rev. B **107**, L100419 (2023).

[36] V. M. Edelstein, Spin polarization of conduction electrons induced by electric current in two-dimensional asymmetric electron systems, Solid State Commun. **73**, 233 (1990).

[37] D. Culcer and R. Winkler, Generation of Spin Currents and Spin Densities in Systems with Reduced Symmetry, Phys. Rev. Lett. **99**, 226601 (2007).

[38] A. Chernyshov, M. Overby, X. Liu, J. K. Furdyna, Y. Lyanda-Geller, and L. P. Rokhinson, Evidence for reversible control of magnetization in a ferromagnetic material by means of spin–orbit magnetic field, Nat. Phys. **5**, 656 (2009).

[39] A. Manchon and S. Zhang, Theory of nonequilibrium intrinsic spin torque in a single nanomagnet, Phys. Rev. B **78**, 212405 (2008).

[40] I. Garate and A. H. MacDonald, Influence of a transport current on magnetic anisotropy in gyrotropic ferromagnets, Phys. Rev. B **80**, 134403 (2009).

[41] R. Peters and Y. Yanase, Strong enhancement of the edelstein effect in $f$-electron systems, Phys. Rev. B **97**, 115128 (2018).

[42] M. Fiebig, Revival of the magnetoelectric effect, J. Phys. D **38**, R123 (2005).

[43] Y. Yanase and M. Sigrist, Superconductivity and magnetism in non-centrosymmetric system: Application to $CePt_3Si$, J. Phys. Soc. Jpn. **77**, 124711 (2008).

[44] Y. Michishita and R. Peters, Impact of the rashba spin-orbit coupling on $f$-electron materials, Phys. Rev. B **99**, 155141 (2019).

[45] A. Georges, G. Kotliar, W. Krauth, and M. J. Rozenberg, Dynamical mean-field theory of strongly correlated fermion systems and the limit of infinite dimensions, Rev. Mod. Phys. **68**, 13 (1996).

[46] M. Potthoff and W. Nolting, Surface metal-insulator transition in the hubbard model, Phys. Rev. B **59**, 2549 (1999).

[47] J. Vahedi, R. Peters, A. Missaoui, A. Honecker, and G. T. de Laissardière, Magnetism of magic-angle twisted bilayer graphene, SciPost Phys. **11**, 083 (2021).

[48] R. Peters and N. Kawakami, Large and small fermi-surface spin density waves in the kondo lattice model, Phys. Rev. B **92**, 075103 (2015).

[49] R. Peters and N. Kawakami, Spin density waves in the hubbard model: A dmft approach, Phys. Rev. B **89**, 155134 (2014).

[50] K. G. Wilson, The renormalization group: Critical phenomena and the kondo problem, Rev. Mod. Phys. **47**, 773 (1975).

[51] R. Bulla, T. A. Costi, and T. Pruschke, Numerical renormalization group method for quantum impurity systems, Rev. Mod. Phys. **80**, 395 (2008).

[52] R. Peters, T. Pruschke, and F. B. Anders, Numerical renormalization group approach to green's functions for quantum impurity models, Phys. Rev. B **74**, 245114 (2006).

[53] R. Peters, N. Kawakami, and T. Pruschke, Spin-Selective Kondo Insulator: Cooperation of Ferromagnetism and the Kondo Effect, Phys. Rev. Lett. **108**, 086402 (2012).

[54] M. A. Ruderman and C. Kittel, Indirect exchange coupling of nuclear magnetic moments by conduction electrons, Phys. Rev. **96**, 99 (1954).

[55] T. Kasuya, A theory of metallic ferro- and antiferromagnetism on zener's model, Prog. Theor. Phys. **16**, 45 (1956).

[56] K. Yosida, Magnetic properties of Cu-Mn alloys, Phys. Rev. **106**, 893 (1957).

[57] J. Neuhaus-Steinmetz, E. Y. Vedmedenko, T. Posske, and R. Wiesendanger, Complex magnetic ground states and topological electronic phases of atomic spin chains on superconductors, Phys. Rev. B **105**, 165415 (2022).